Wettability-dependent Wave Velocities and Attenuation in Granular Porous Media

Jimmy X. Li[1], Reza Rezaee[1], Tobias M. Müller[2,3], Mahyar Madadi[4], Rupeng Ma[3]and Mohammad Sarmadivaleh [1]

[1]Western Australian School of Mines, Curtin University, Kensington, WA 6151, Australia.
[2]Department of Seismology, Centro de Investigacion Cientifica y de Educacion Superior de Ensenada, 22860 Ensenada, BC, Mexico.
[3]School of Earth Sciences and Engineering, Hohai University, Nanjing 211100, China.
[4]School of Mathematics and Statistics, The University of Melbourne, Parkville, VIC 3010, Australia.

Key Points:

- The first experimental investigation of wettability effect on the wave phenomena in granular porous media with variable water saturation.
- The wettability affects the wave velocity and attenuation by controlling the spatial distribution of fluids.
- The wave scatterings in granular porous media are linked to wettability and saturation.

Corresponding author: Jimmy X. Li, Jimmy.Li@postgrad.curtin.edu.au, 26 Dick Perry Avenue, Kensington, WA 6151, Australia.

Abstract

Understanding wave propagation in granular sediments is important for subsurface characterization. The presence of fluid and wettability condition result in additional complexities. While it is known that wave propagation in dry granular porous media is dominated by the presence of force chains, their influence in (partially) saturated granular porous media with different wettability conditions remains largely unexplored. To make progress in this direction, we design laboratory experiments by combining core flooding and ultrasonic measurement in glassbead packings that are chemically treated to alternate the wettability. The P- and S-wave velocity-saturation relation and attenuation-saturation relation are obtained from the waveforms for both water- and gas-wetting samples. The results show that there is a transition from an attenuating but stable P-wave pulse at low and moderate saturation to a set of incoherently scattered waves at high saturation. The incoherent scattering in the gas-wetting case is negligibly small, whereas it is more pronounced in the water-wetting case. We conclude that only if water wets the grains, can the liquid enter the grain contacts. These liquid bridges are thought to locally reinforce the force chains and to increase their characteristic length scale. This leads to an increase in P-wave velocity and promotes incoherent scattering since the ratio of dominant wavelength to characteristic length scale decreases. In the gas wetting case, however, the presence of gas prevents the water from direct contact with the glass beads and therefore stops the formation and growth of the liquid bridges within the force chain network.

Plain Language Summary

The distinction of waveforms from the acoustic measurement of granular porous media with different wettability demonstrates that wettability has a significant influence on wave propagation. This is because the spatial distribution of the fluids is controlled by wettability. Only if the sample is water wetting, the liquid can occupy grain contacts. These liquid-reinforced grain contacts result in higher velocities, less attenuation. In addition, the spatial arrangement of the liquid-reinforced grain contacts is thought to change the characteristic length scale of the force chains. This can lead to the scattering of wave pulses when their dominant wavelengths are comparable to the characteristic length scale.

1 Introduction

Since granular porous media define zones with high porosity and permeability they are important for freshwater aquifer characterization, oil and gas production, and CO_2 geo-sequestration. Hence, there is a wide genre of scientific interests in the properties of granular porous media, including their acoustic properties (C.-h. Liu & Nagel, 1992; Melosh, 1996; Scott, 1996; P. A. Johnson & Jia, 2005; Parra et al., 2006; Moebius et al., 2012; Lo & Sposito, 2013; Güven et al., 2018). In the context of groundwater exploitation and exploration geophysics, soft and unconsolidated sediments (e.g. soil and sand packings) in the subsurface are often conceptualized as fluid-saturated granular porous media. In particular, for the interpretation of sonic and seismic data it is important to understand their overall elastic properties, velocity dispersion, and attenuation mechanisms (Anthony & Marone, 2005; Daniels & Hayman, 2008; T. Dutta et al., 2010).

It is known that for porous media saturated with more than one fluid the wave velocity is not only dependent on the saturation, i.e., the volumetric proportion, but also dependent on the fluid distribution, i.e., the geometrical arrangement and length scales of fluid pockets. In this regard, there have been several experiments to study the velocity-saturation-relation (VSR) in various lithologic rocks with mixed liquid-gas saturation (Murphy III, 1984; Cadoret et al., 1995; Lebedev et al., 2009; Alemu et al., 2013; Lopes et al., 2014). These VSR can be often constrained by the two end-member models of patchy and uniform saturation. They correspond to the upper bound and lower bound velocities de-

scribed by the Gassmann-Hill (GH) and Gassmann-Wood (GW) equations, respectively (Toms et al., 2006). Similar experiments for granular porous media are not known. Even the applicability of the GW and GH bounds in partially saturated granular porous media remains unclear. Nonetheless, it is known that wave velocities are strongly different in dry and saturated granular porous media (Job et al., 2008; Brunet et al., 2008; Griffiths et al., 2010). Therefore, one can expect a pronounced signature of partial saturation to be present in granular porous media as well.

As far as velocity dispersion and attenuation in partially saturated rocks are concerned, there are multiple models to account for wave-induced-fluid-flow (WIFF), which is thought to be a relevant dissipation mechanism caused by the relative motion of solid and fluid (White, 1975; N. Dutta & Odé, 1979; Santos et al., 1990; Mavko & Mukerji, 1998; D. L. Johnson, 2001; Müller & Gurevich, 2004; Lo et al., 2005; Ba et al., 2011; Sun et al., 2018). These models are used to interpret observed VSRs that do not follow either the GH or GW bounds, but show trends in between these bounds. These WIFF models also allow us to interpret the attenuation-saturation relation (ASR) (Qi et al., 2014; J. Liu et al., 2016). While it is known that waves in granular porous media become attenuated, one may expect additional attenuation in partially saturated granular porous media (Brunet et al., 2008). However, the precise nature of WIFF in granular porous media is unknown, and therefore the applicability of one of the above-mentioned models remains questionable.

The presence of two fluids inevitably implies that two-phase flow concepts such as capillarity and wettability become relevant. For example, Qi et al. (2014) find that capillarity stiffening may result into higher wave velocities and accordingly modify the GW bound based on ideas earlier suggested by Nagy and Blaho (1994) and Tserkovnyak and Johnson (2003). Lo et al. (2017) discover the dynamic response of the water retention curve (relationship of capillary pressure and water saturation) during water drainage in unsaturated porous media under acoustic excitation. The wettability as an interfacial phenomenon is thought to be a key factor controlling the spatial distribution of fluids. Their location and displacement will have significant influence on the capillary pressure, relative permeability, and water-flooding performance (Anderson, 1987; Anderson et al., 1987a, 1987b; Bultreys et al., 2016; Khishvand et al., 2017; Hu et al., 2017).

However, in none of the above-mentioned studies, the wettability of the porous media has been considered. Ignoring the wettability impact on wave propagation may lead to errors and misinterpretation of experimental and field test results. Therefore, in an attempt to understand the effect of wettability on waves velocities, we aim at experiments in an idealized porous medium, in which we can have full control of the wettability. For this purpose, we choose glass bead packings as a particular simple representation of a granular porous medium.

Although there are a lot of similarities between granular porous medium and rigid porous medium and some poroelastic theories may be applicable to the granular porous medium, the grains in granular porous medium have additional degree of freedom compared to the solid frame of consolidated rigid porous media. In non-cohesive granular porous media under external stress, some grains are load-bearing, others not. This results in an inhomogeneous pattern of load-bearing grains, the so-called force chain networks. Force chain networks can be directly observed by photo-elastic visualization experiments (Howell et al., 1999; Owens & Daniels, 2011; Ladd & Reber, 2020).

Since the contact force chain network bears the strongest stress on the direction of the compression, it dominates the mechanical properties of granular porous media, including the elastic response to the external disturbance such as acoustical perturbation (C. M. Sayers, 2021). When the granular porous medium is saturated by two immiscible fluids, the grain contacts are always occupied by the wetting fluid because of the capillary action, while the non-wetting fluid is forced into the relatively larger pores (Anderson

et al., 1986). Such a wettability-dependent spatial distribution of fluids is most likely to affect the structure of the force chain network. Different from the dry Hertzian contacts, the presence of the liquid bridges in the grain contacts (i.e. the water bridges in the water-wetting sample) induce the elastohydrodynamic collision of grains under ultrasonic frequency, which consequently increase the stiffness of the contact, enlarge the force chain network and therefore increase the characteristic length of the force chains (Davis et al., 1986; Job et al., 2008).

In this paper, we explore the wettability effect on the wave propagation in the (partial) saturated granular porous media by the experiments combining acoustic measurement and core flooding. We first present the experiment setup and results. The waveform of the P- and S-wave on each step of incremental water injection (increase of water saturation) are recorded for both water-wetting and gas-wetting glass bead packings. The velocity-saturation-relation (VSR) and attenuation-saturation-relation (ASR) are extracted from the waveforms. Then, the wettability dependent scattering patterns are identified for two samples with different wettability. A wettability-dependent characteristic length of the force chains is used to interpret the wave scattering observations and the piece-wise function of effective bulk and shear moduli are proposed to simulate the transition from coherent wave in dry or low saturation to incoherent wave in high and full saturation.

2 Experimental Setup

The experimental setup consists of a poly-carbonate cylinder (15.5 mm inner diameter and $48-52$ mm length) packed with spherical glass beads with a quasi-identical diameter of 200 ± 50 μm and two piston piezoelectric acoustic transducers mounted on the two ends. This is the typical configuration to carry out acoustic measurements in granular materials (P. A. Johnson & Jia, 2005). The fluid can be injected through the inlet line and the displaced fluid exits through the outlet line (Figure 1). Olympus V103 and V153 piezoelectric transducers with broadband frequency range $0.2-2$ MHz and 1 MHz nominal (center) frequency are used to generate and receive P- and S-wave pulses, respectively. A uniaxial pressure of about 150 kPa is applied on the outside faces of the transducers to guarantee dense packing.

To indicate the wettability the contact angle is measured. The water droplets are applied on the original glass surface and the Quilon-C treated surface, respectively, in the air environment. The measured contact angle is on a water-air-glass interface is 7.64°, which is far less than 90° indicating that the pure, untreated glass beads are strongly water-wetting (Figure 2). The water is incrementally injected into the packing through the inlet line with an approximate flow rate of 0.7 ml/s. The acoustic measurement is conducted after each incremental injection. The change of water saturation is precisely captured by measuring the weight of the sample.

The same injection-measurement procedure is performed on the glass bead packing when the wettability is altered in order to have gas wetting glass beads. Quilon-C in isopropyl alcohol solution is used to alter the wettability of the original water-wetting glass beads to be gas-wetting by following the same procedures outlined in the literature (Garrouch & Sharma, 1995). The chemical contains C-14-C-18 fatty acids with chromium, which bonds the negatively charged glass bead surface rendering a gas-wetting (hydrophobic) thin coating on the spheres. An advantage of such treatment is that there is little impact on the porosity of the fully saturated porous medium (Garrouch & Alikhan, 1997). We find that the porosity of glassbead packing changes from 38.5% as original hydrophilic condition to 37.5% as processed hydrophobic condition. The hydrophobicity or gas-wetting condition is confirmed by a 105.5° measured contact angle on the water-air-glass interface after the Quilon-C chemical treatment (Figure 2).

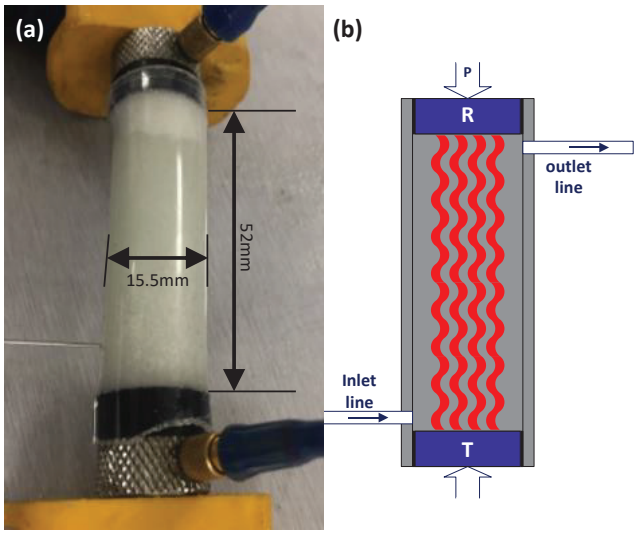

Figure 1. (**a**) Real and (**b**) schematic experimental set-up for conducting acoustic measurement during the water-air core flooding in the glass bead pack under axial pressure P. T and R denote the piezoelectric transmitter and receiver, respectively.

While the porosity and permeability are not significantly changed due to the chemical treatment, the mechanical properties are expected to change. In the case of water-wetting glass bead packing, the sample can be thought as uncoated, only held together by the enclosure of sleeve and the uniaxial compression applied. However, in the gas-wetting glass bead packing, the water-repellent coating and the possible residual chemical deposition on the glass beads as demonstrated in Figure (2b) act as coating layers. They strengthen the entire stiffness of the gas-wetting glass bead packing (Dvorkin et al., 1991, 1994). This is confirmed by the observation that the P-wave velocity of dry gas-wetting glass bead packing is higher than the value of dry water-wetting sample (Figure 5 and 6).

3 Experimental Results

3.1 Water-wetting Case

Seismograms of P- and S-waves are recorded separately for the water-wetting sample for each saturation step (Figure 3). We observe that in the P-wave transmission experiment (Figure 3a) there is a clear transition from a stable coherent wave pulse towards a set of incoherent scattering waves with shorter wavelengths for increasing water saturation. With incremental water injection, initially the traveltime of the first arrival slightly increases and the amplitude decreases slowly until a critical water saturation $S_c \approx 89\%$ is reached. Beyond this critical saturation the traveltime becomes very short and the amplitude increases sharply. For the S-wave transmission experiment, there is only one coherent pulse recognizable whose traveltime increases slightly with the increase of water saturation. Nevertheless, the P-wave arrival is visible on the S-wave measurement at low and intermediate water saturation (Figure 3b).

3.2 Gas-wetting Case

The gas-wetting glass beads are obtained from the original water-wetting beads treated by the wettability alteration agent Quilon-C. Better contact between glass beads is ex-

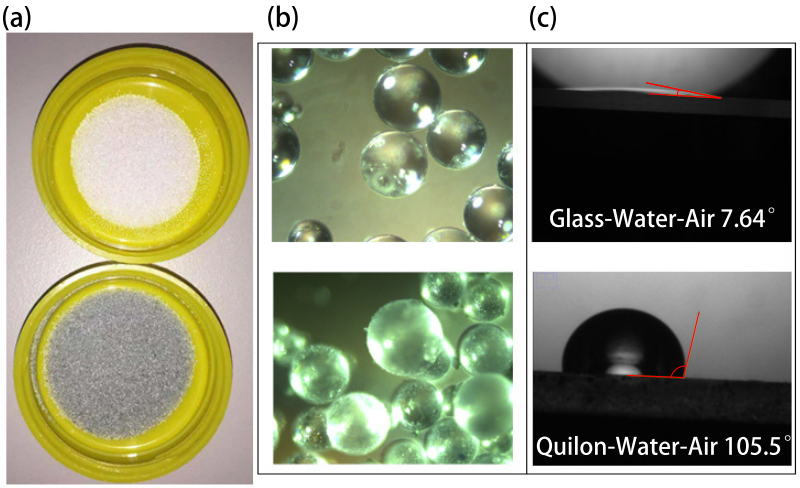

Figure 2. (**a**) Original glass bead sample (top) appearing in shiny white color and the Quilon-C treated glass bead sample (bottom) in dark green color; (**b**) microscopy images of the original glass beads and treated beads; (**c**) the corresponding contact angle of water droplet on original glass surface (top) is 7.64° and on the processed glass surface after Quilon-C chemical treatment (bottom) is 105.5°.

pected after the treatment. This is indeed corroborated since we observe higher amplitude and higher velocity for dry gas-wetting glass bead packing compared to the original water-wetting one. However, with the increase of water saturation, the gas wetting packing exhibits a strong damping effect and the waveforms of both P- and S-wave become attenuated drastically (Figure 4). The increase of water saturation stops around 93%-94% in the standard water flooding procedure with about 6% residual gas saturation. After a three-fold increase of the injection pressure, we spot some of the suspected scattered P-waves after the critical water saturation $Sc \approx 98\%$, though the amplitude is very small (Figure 4a). The gas as wetting fluid phase is trapped inside the grain contact and is hardly displaced by the water in the standard water injection process. However, the increased injection pressure may overcome the capillary pressure and thereby push the non-wetting water into some of the grain contacts.

4 Wettability Impact on the Velocity and Attenuation

The inferred velocity-saturation relation (VSR) of both P- and S-wave transmission experiments are plotted in Figure 5 and 6 for the water-wetting and gas-wetting samples, respectively. The results are compared with the Gassmann-Wood limit (lower bound for uniform saturation) and Gassmann-Hill limit (upper bound for patchy saturation), where the detailed formulas are given in Appendix A. The predictions of the Biot theory, i.e., for a fully saturated porous medium are also provided for reference. The parameters of the samples are listed in Table 1. In addition, we calculate the attenuation-saturation relation for both transmission experiments. The attenuation is obtained via the spectral-ratio method with key formulas in Appendix B. The results are plotted in Figure 7.

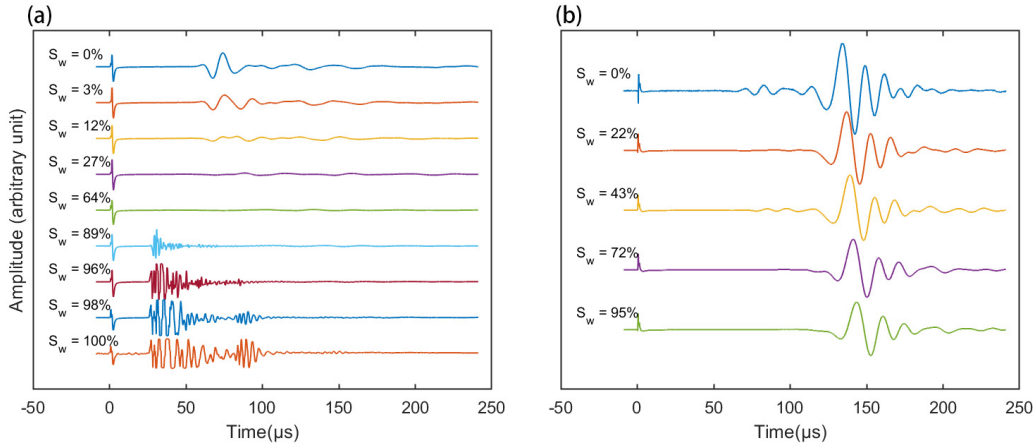

Figure 3. Recorded waveforms of (**a**) *P*-wave and (**b**) *S*-wave after incremental injection for water-wetting glass bead packing. The small peak at the t=0 is the cross-talk signal during the pulse generation.

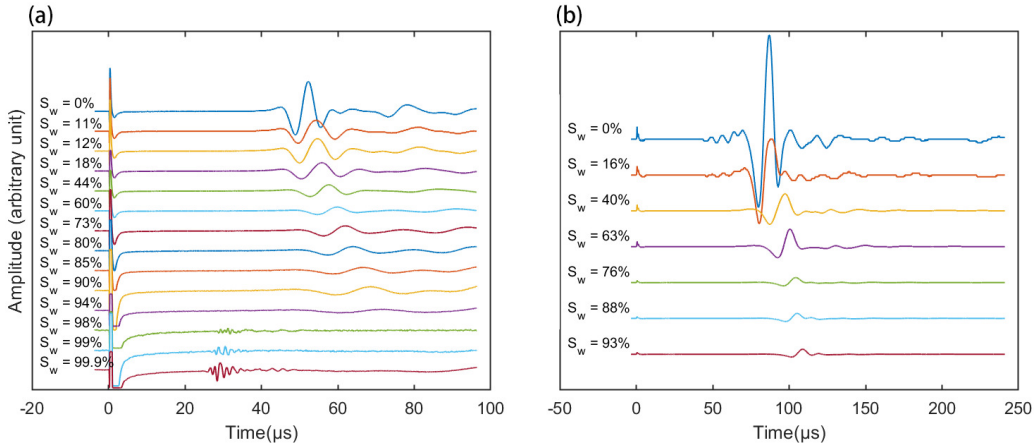

Figure 4. Recorded waveforms with incremental water injection for gas-wetting glass bead packing: (**a**) *P*-wave; (**b**) *S*-wave transmission experiments.

4.1 Water-wetting Case

For the water-wetting sample, water tends to occupy the glass bead surface and the grain contacts as soon as the fluid is fingering through the inter-granular voids. This favors the generation of capillary bridges (pendulum rings made of water). Initially, such capillary bridges may only appear in the finest and smallest pores. The water then quickly occupies the relatively large pores. At low- to intermediate water saturation, the capillary bridges are not fully established in all grain contacts. Therefore, the force chains are thought to form a discontinuous pattern like schematically indicated in inset of Figure 5. Then the *P*-wave VSR is closer to the prediction of Gassmann-Wood bound. At the same time, the attenuation of the *P*-wave (Figure 7a) becomes higher with increasing water saturation but the attenuation of the *S*-wave (Figure 7b) is less affected by the change of water saturation. Once the water saturation reaches a critical saturation (i.e., $S_c \approx 89\%$) and beyond, the force chains under ultrasonic frequency become reinforced and the grain contacts saturated by water form in a continuous percolating pattern (inset of Figure 5).

Table 1. Parameters of Glassbead Packing and the Injected Water

Water	
Density, ρ_w	997 kg/m^3
Bulk Modulus, K_w	2.25 GPa
Viscosity, μ_w	1 cP
Gas (air, 25 °C)	
Density, ρ_g	1.18 kg/m^3
Bulk Modulus, K_g	0.142 MPa
Solid	
Density, ρ_s	2455 kg/m^3
Bulk Modulus, K_s	37 GPa
Grain Diameter,d	200 μm
Water-wetting Matrix	
P- Wave Velocity, V_p	963.504 m/s
S- Wave Velocity, V_s	466.36 m/s
Porosity, ϕ	0.385
Tortuosity†, T	1.8
Permeability‡, κ	3.37×10^{-11} m^2
gas-wetting Matrix	
P- Wave Velocity, V_p	1295.24 m/s
S- Wave Velocity, V_s	782 m/s
Porosity, ϕ	0.375
Tortuosity†, T	1.83
Permeability‡, κ	3×10^{-11} m^2

† Estimated by $T = \frac{1}{2}(1 + 1/\phi)$ (Berryman & Thigpen, 1985).
‡ Kozeny-Carman Permeability $\kappa = \frac{\phi^3}{180(1-\phi)^2}d^2$ (Xu & Yu, 2008).

This interstitial liquid-induced structural change of the force chains has paramount impact on the velocity and the attenuation. On the one hand, it leads to higher effective elastic moduli (both bulk modulus and shear modulus) of matrix frame. Since the composite density does not change appreciably, the corresponding P- and S-wave velocities at higher saturation are larger compared to the Gassmann theory predictions (Figure 5). On the other hand, the overall growth of the force chain network is accompanied with a local clustering of grains connected via capillary bridges. These clusters, in turn, can be characterized by a characteristic length which exceeds the individual grain size. Once the characteristic length becomes comparable to the P-wavelength, the notion of an effective medium is no longer valid. Instead, one expects that the P-wave are elastically scattered at the clusters. This could explain the emergence of the incoherent wave pulses seen in Figure 3. Given that the frequency range of the piezoelectric transducer is $0.2-2$ MHz, the P-wavelength ranges from $1-10$ mm for either water-wetting or gas-wetting samples in (near) full water saturation condition. However, the diameters of the glass beads are much smaller,$d = 0.2 \pm 0.05$ mm. If the characteristic length of the force chains is short-ranged ($\xi \sim d$) due to the gas filled grain contacts, there should

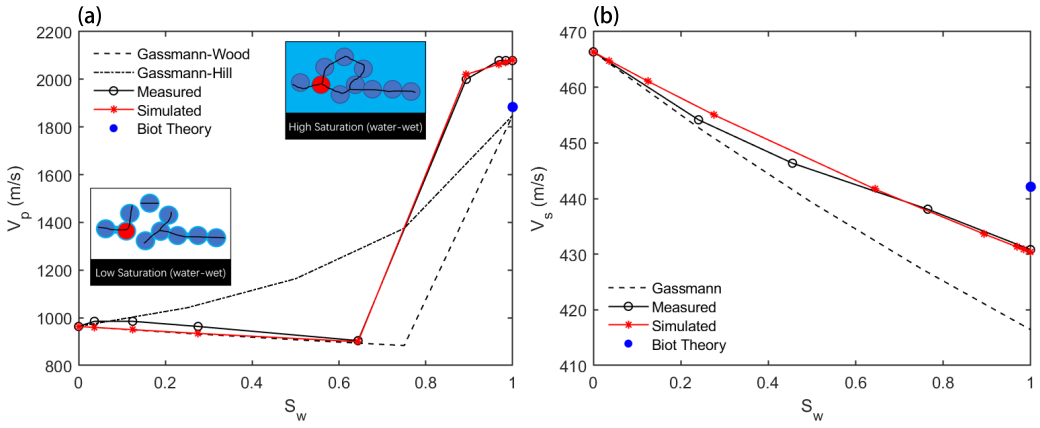

Figure 5. The measured velocity-saturation relation in water-wetting glass bead packing is compared with Gassmann-Wood and Gassmann-Hill theoretical predictions for (**a**) P-Wave and (**b**) S-Wave. As reference, Biot theory is used for calculation of the velocities of sample under full water saturation. The inset cartoons illustrate the network of force chain (black solid line) in low and fully saturated samples.

be little incoherent signals and a stable P-wave pulse is propagating. However, the observation of the incoherently scattered waves in the water-wetting sample is suggestive for the existence of long-range characteristic length ($\xi \sim 5 - 10d$).

The appearance of these incoherently scattered waves is also clearly marked as a negative $1/Q_p$ in the P-wave attenuation-saturation relation (Figure 7a). The negative value is a consequence of using the spectral ratio method to determine Q. It essentially consists in dividing the amplitude spectrum of a waveform by a reference amplitude spectrum (i.e., the signal in an aluminum core with the same length as the sample). This reference amplitude spectrum in shown in Figure 8b (black line). The amplitude spectrum corresponding to the first period of a scattered wave in the water-wetting sample has two peaks (Figure 8b, red line). The center frequency that corresponds to the first peak (#1 in Figure 8b) is lower than the center frequency of the reference amplitude spectrum. Computing the spectral ratio at this center frequency yields to a positive Q value. Conversely, computing the spectral ratio at the center frequency of the second peak (#2 in Figure 8b) yields to a negative Q value. The changes in the force chain network due to the injection of the liquid bring the amplitude spectrum a bi-modal pattern, which contains not only low-frequency coherent waves but also high-frequency incoherent scattering components (Figure 9a). These scattered waves are associated with a negative $1/Q$. In this sense, the Q factor does not quantify the amplification of a pulse but is an indication of the change of signal character.

The Gassmann-Wood predictions match the measured P-wave velocity reasonably well at low- to intermediate water saturation as long as the saturation is below the critical water saturation S_c. At a water saturation beyond S_c, the force chain network is enriched with unrelaxed grain contacts, where local pressure gradients induced by the wave are not equilibrated. Such a scenario resembles the high-frequency unrelaxed frame concept developed by Mavko and Jizba (1991) and described by the Mavko-Jizba relation. The basic idea is that the non-equilibrated wave-induced pressure perturbation at grain contact is incorporated in form of high-frequency unrelaxed "wet-frame" moduli K_{uf} and μ_{uf}. These moduli are higher compared to the moduli at low frequencies when the pressure gradients are equilibrated. We find that the Mavko-Jizba relations work well to predict the P- and S-wave velocities of the fully saturated water-wetting sample as the wa-

ter occupies the grain contacts to form a "wet-frame". By taking advantage of the two end velocities (dry and full saturation), we are able to simulate the P-wave velocities at high saturation ($S_w \geq S_c$) and S-wave velocities by the Voigt averaged elastic moduli:

$$K = \begin{cases} K_{GW}; & \text{if } \mathrm{S_w} < \mathrm{S_c} \\ K_d(1-S_w) + K_{MJ}S_w & \text{if } \mathrm{S_w} \geq \mathrm{S_c} \end{cases} \tag{1}$$

$$\mu = \mu_d(1-S_w) + \mu_{MJ}S_w \tag{2}$$

where the K_{GW} are Gassmann-Wood limit of the bulk modulus of the partially saturated sample, K_{MJ} and μ_{MJ} are the bulk and shear moduli of the fully saturated sample by Mavko-Jizba relations, K_d and μ_d are the bulk and shear moduli of the drained (dry) sample. The simulated velocities mathch the measured velocities very well as demonstrated in Figure 5. We list the relevant formulas in Appendix A.

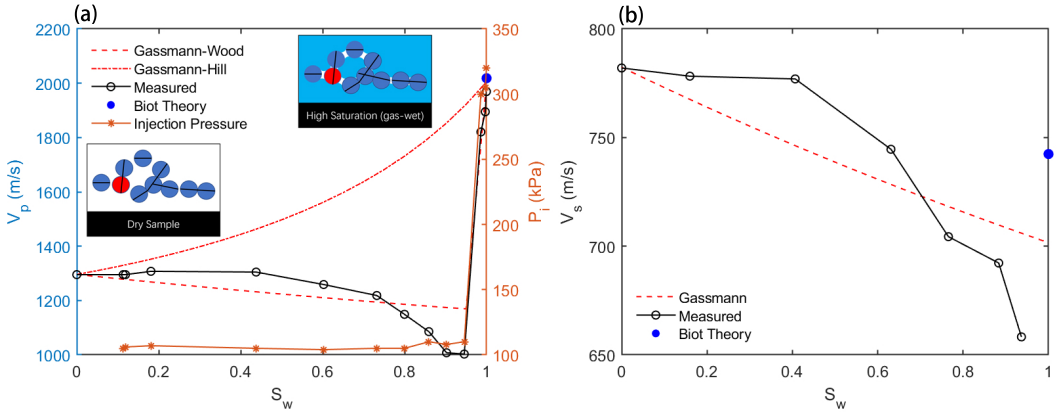

Figure 6. Velocity-saturation relation in gas-wetting glass bead packing vs Gassmann-Wood and Gassmann-Hill predictions for (**a**) P-Wave and (**b**) S-Wave. The last three measurements in high water saturation are obtained after increasing 300% injection pressure P_i. The inset cartoons demonstrate the network of force chain (black solid line) in dry and high to near fully saturated samples.

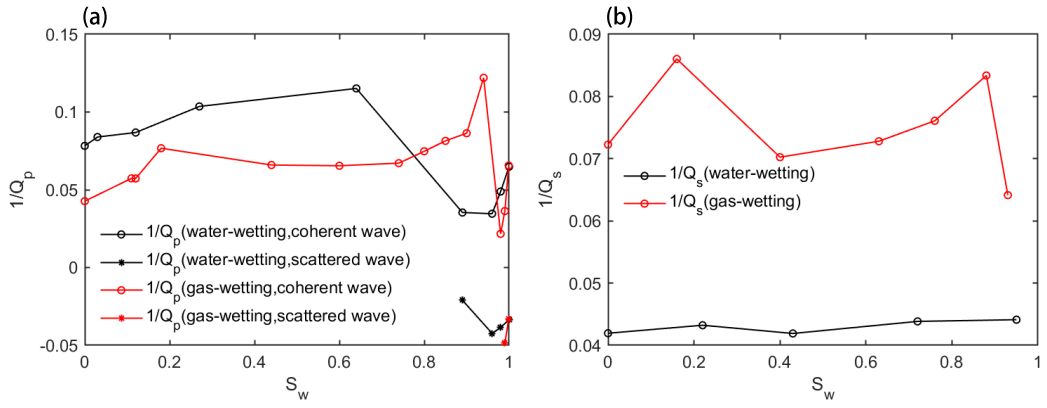

Figure 7. Attenuation-saturation relation of (**a**) P-wave and (**b**) S-wave for both water-wetting and gas-wetting samples.

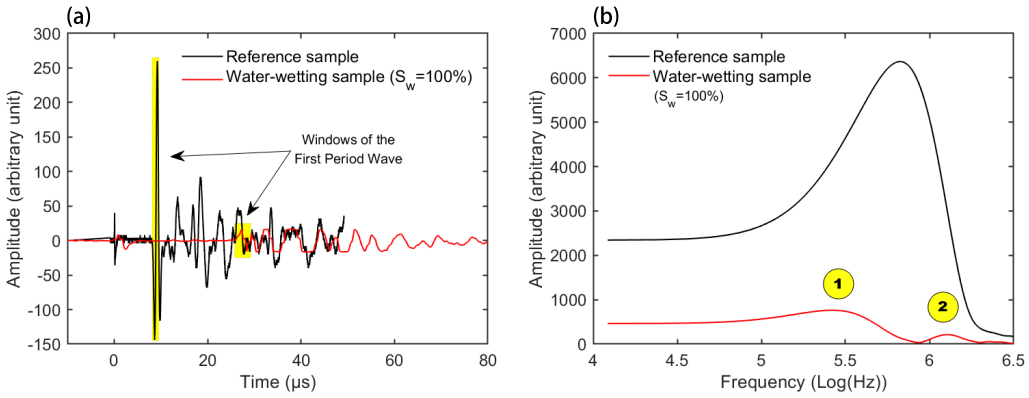

Figure 8. (**a**) The waveforms through the reference sample (aluminum dummy core) and water-wetting sample with 100% water saturation where the time windows of the first period of waveforms are selected (shading highlight) for calculating the amplitude spectrum in each sample; (**b**) the corresponding spectra by Fourier transform where two peaks are produced in the spectrum of signals in fully saturated water-wetting sample.

4.2 Gas-wetting Case

Our hypothesis is that only the fluid between the grain contacts has significant impact on the force chain network and therefore on the effective bulk moduli of the matrix frame. For the gas-wetting case, air as wetting-fluid tends to occupy the grain contacts while water is forced into the relatively large interstitial pores from the beginning to the end of the water injection (inset of Figure 6). Since the bulk modulus of the air in the grain contacts of the gas-wetting glass beads is negligibly small we expect no significant change of the structure of the force chain network and the effective moduli of the matrix frame during the water flooding. The measured P-wave VSR coincidentally agrees with the predictions of Gassmann-Wood limit but is far away from Gassmann-Hill prediction. This indicates that the two immiscible fluids tend to be in a homogeneous mixing condition rather than forming patchy fluid pockets (Figure 6).

The water saturation stops increasing at about 93-94% in the normal water flooding procedure with about 6% residual gas saturation for the gas-wetting sample. Only when we increased the injection pressure by about 300% in an attempt to overcome the capillary pressure, the non-wetting water was pushed into some of the grain contacts. In our interpretation, this should lead to a force chain reinforcement. This is supported by the observation of small amplitude "scattered" waves, which in fact contain both coherent part and incoherent part (Figure 9b). Their P-wave attenuation obtained by the spectral-ratio method is as similar to the scenario of the water-wetting sample.

4.3 The Role of Wettability in P-wave Transmission

There is only one coherent pulse observed in the S-wave transmission experiments regardless the saturation condition and the wettability of the samples. In contrast, in the P-wave transmission experiments, there is a transition from the coherent P-wave pulse in the dry samples to the incoherently "scattered" waves in the samples with high water saturation.

The amplitude spectra of P-waves in the fully water-saturated samples are plotted in Figure 8. We observe that the water-wetting spectra contains a low-frequency part and a high-frequency part. Similar experimental observations are reported by Güven et

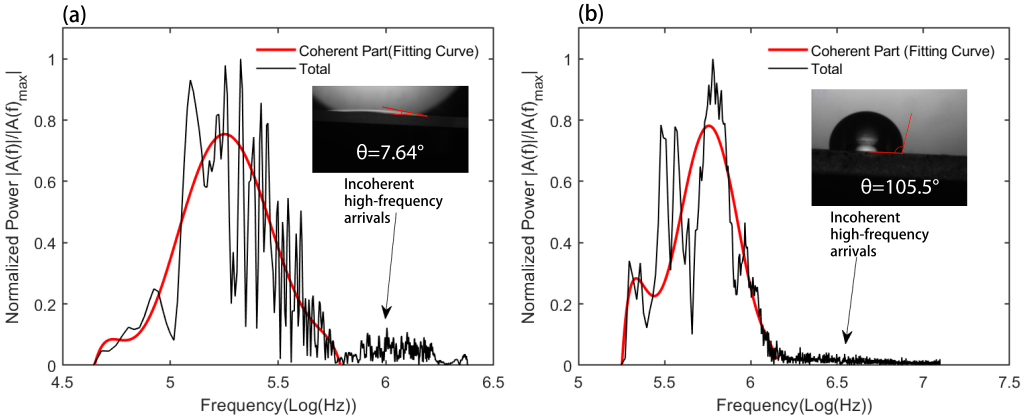

Figure 9. The Amplitude spectra A(f) normalized by the maximum value for the fully saturated (**a**) water-wetting and (**b**) gas-wetting glass bead packings. The insets of figures show the contact angle of water droplet on the glass-air interface.

al. (2018) and Jia et al. (1999). However, the incoherent arrivals in the spectra of gas-wetting sample are rare and small. We project that the fluid in the grain contacts plays a crucial role in the continuity of the force chains, where the liquid promotes the development of long force chains as in the water-wetting glass bead packing, but the gas, i.e., air restrains the extension of the force chains as in the gas-wetting glass bead packing. In this way, the wettability is identified to have significant impact on the force chain network by controlling the intergranular fluid distribution, which further determine the wave velocity, attenuation and scattering.

5 Discussion

5.1 Path Effect on the Acoustics of Porous Granular Media

When the wetting phase fluid is injected into the dry granular porous medium, it percolates through the pore space and occupies relatively small voids (i.e., grain contacts) in sequence. In this way, the force chains are extended and re-organized. However, it is unlikely that the percolation process proceeds such that a homogeneous force chain pattern (FCP) is generated. This should be especially true when the capillary pressure is small and the impact of gravity on the fluid distribution become considerable. In the following we explore some of the factors that may be responsible for the generation of heterogeneous FCPs, which in turn could explain the wavefield signatures observed from ultrasonic experimentation.

We hypothesize that heterogeneous FCP may occur during the injection such that the notion of an effective medium is no longer valid and instead the heterogeneous FCP gives rise to preferential wave (ray) paths, i.e., the path effect. To verify this hypothesis and investigate the path effect in porous granular media, we repeat the experiment as described in Section 2 but introduce two changes. First, we inject decane instead of water as the wetting phase fluid. The benefit of decane over water is that the decane has smaller interfacial tension in air ($\sigma = 24.47 mN/m$) compared to water($\sigma = 72 mN/m$) (Rolo et al., 2002). The glass bead surface has similar wettability to the decane as to the water in the air with a contact angle of less than 10° so that the capillary pressure $P_c = 2\sigma \cos\theta / r$ for the decane-air system is only about 1/3 of the water-air system. Hence, the interplay between capillary forces and gravity (the sample in Figure 1 is oriented hor-

izontally) should be more pronounced, thereby generating a more favorable condition for FCP generation.

Second, we use a shorter sample of length $L = 2.8cm$ (roughly half of the length of the original sample; Figure 1). Because the shorter sample is used in the decane injection experiment, a portion of the heterogeneous decane saturation front is likely to reach the receiver early-on in the fluid injection experiment, say at low to moderate decane saturation. This is indeed observed experimentally (Figure 10a). It is thought that this heterogeneous saturation front creates different ray paths for ultrasonic waves (Figure 10b), thereby increasing the level of heterogeneity of the FCP. Specifically, the continuously decane saturated regions constitutes a distinguished fast ray path along which the high frequency waves travel. Since the FCP in the saturated regions is thought to be accompanied with larger characteristic lengths, these fast rays are scattered at clusters. The dry and the low saturation regions correspond to slow ray path along which mainly the low-frequency part of the broadband waves propagates. This leads to a deformation of the wave front and bias towards larger velocity by picking the first break as illustrated in Figure 10b. Such deformed wave front accounts for the mechanism of fast path dispersion or velocity shift (Cadoret et al., 1995; Mukerji et al., 1995). This could explain the recorded P-waveforms at intermediate saturation (i.e., $S_o = 58\%$ and $S_o = 64\%$) in the decane injection experiment, where two types of wave arrivals with different frequencies are recorded in the same wave train (Figure 11).

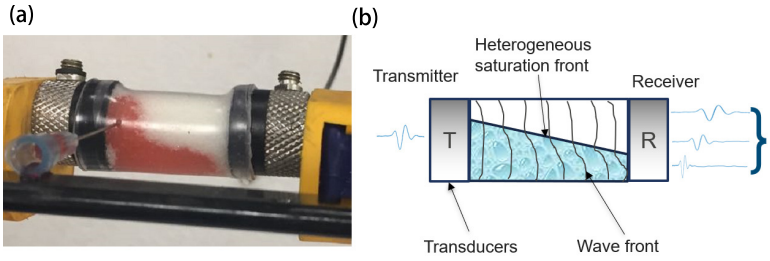

Figure 10. (**a**) Different ray paths are produced during the injection of liquid into the short sample (L=2.8cm). (**b**) This schematic shows the path effect on the receiving signals with broadband frequencies where the short wavelength (high-frequency) wave tends to follow the fastest ray path.

5.2 Effect of Micro-slip Between Grains

It is worth noting that the velocities of both P- and S-wave drop to values lower than the Gassmann predication at high saturation (from about 75% to 93%) in the gas-wetting sample but not in the water-wetting sample (Figure 6). This drop might be explained by micro-slip (sliding) between glass beads as suggested by Makse et al. (2004) and Langlois and Jia (2014). This leads to an increase of the tangential friction (dissipation) since we see a similar pattern of increasing attenuation in both P- and S-wave at moderate to high water saturation in the gas-wetting sample (Figure 7). Such micro-slip also results in a drop in the velocities where the attenuation increases. The occurrence of micro-slip due to the grain sliding may be dependent on the wettability and water saturation. A further investigation will be required to answer this question.

5.3 Comparison with Literature

As shown in the experimental results section, we observe a dramatic change in the waveforms during the change of the fluid saturation in porous granular media. It is in-

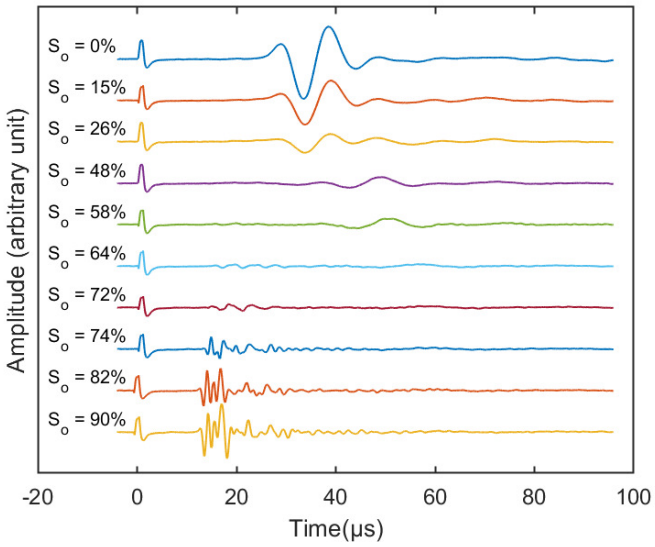

Figure 11. Recorded P-waveforms with incremental decane (oil) injection for shorter glass-bead packings (L=2.8cm). Two types of signals with different frequencies are recorded in the same wave trains at intermediate saturations (i.e. $S_o = 58\%$ and $S_o = 64\%$)

teresting to note that a similar phenomenon is documented by C. Sayers and Dahlin (1993) (their Figure 12). The time-lapse waveform changes from high-frequency (short-period) arrivals when the sample is in the state of a cement paste (suspension of cement articles in water) to low-frequency (long-period) waves when sample becomes a cemented solid (saturated porous media). These waveform changes are caused by the structural changes during hydration and, compared to our results, the transition of the acoustic waveform has a reverse sequence. Since in the cement paste the interconnected chains of cement particles develop as a function of time, their observations may relate to our interpretation in terms of the reinforced force chains due to the presence of the intergranular fluid.

6 Conclusions

The velocity- and attenuation-saturation relations and P-wave scattering patterns in the water-wetting and gas-wetting granular porous media examined here show distinct characteristics. This indicates that the wettability has a significant impact on the wave propagation in the granular porous medium. We explain these characteristics in terms of wettability-dependent force chain network alterations. In particular, the effective elastic moduli and the characteristic length of force chain network are altered during the water injection. The dry granular porous medium, as an extreme example, where all pores are saturated by air, has a short-range characteristic length. It behaves as an effective medium in which a stable pulse waveform is observed. For partial saturation, only if the water wets the grains, the liquid can intrude the small grain contacts. Therefore, the grain contact-filling fluid as wetting phase (i.e., water) results in the development of the longer-range force chains and higher effective moduli. This appears to be a plausible explanation of the wave velocities, that exceed the prediction of the Gassmann theory, and the appearance of shorter pulses comprising a more complex wave train.

Appendix A Gassmann-Wood and Gassmann-Hill limits for partially saturated sample

The velocity of the P- and S-wave for the sample saturated by a single fluid can be calculated as,

$$V_p = \sqrt{\frac{K + \frac{4}{3}\mu}{\rho}}; \tag{A1}$$

$$V_s = \sqrt{\frac{\mu}{\rho}}; \tag{A2}$$

K: bulk modulus of the fully saturated sample
μ: shear modulus of the fully saturated sample
ρ: density of the fully saturated sample

The K and μ can be derived by the Gassmann equations,

$$\frac{K}{K_s - K} = \frac{K_d}{K_s - K_d} + \frac{K_f}{\phi(K_s - K_f)} \tag{A3}$$

$$\mu = \mu_d \tag{A4}$$

K_s: bulk modulus of solid
K_d: bulk modulus of the drained matrix (dry) frame
K_f: bulk modulus of fluid
ϕ: porosity
μ_d: shear modulus of the drained matrix (dry) frame

Gassmann-Wood lower bound limit applying the Wood law to determine the effective fluid bulk modulus K_f which can be further applied to determine the bulk modulus of partially saturated sample ($K_{GW} = K$) by Eq. (A3) and the velocity by Eq. (A1),

$$\frac{1}{K_f} = \frac{S_w}{K_w} + \frac{1 - S_w}{K_g} \tag{A5}$$

S_w is the water saturation; K_w and K_g are the bulk moduli of the water and gas, respectively.

Gassmann-Hill upper bound limit uses the Hill average bulk modulus of the partially saturated sample K which can be further used in to calculate the velocity by Eq. (A1),

$$\frac{1}{K + \frac{4}{3}\mu} = \frac{S_w}{K_1 + \frac{4}{3}\mu} + \frac{1 - S_w}{K_2 + \frac{4}{3}\mu} \tag{A6}$$

K_1 , K_2 are the bulk moduli of the sample fully saturated by water and gas, respectively.

In either Gassmann-Wood or -Hill limit calculation, the density of the composite partially saturation sample is,

$$\rho = \rho_s(1 - \phi) + (\rho_w S_w + \rho_g - \rho_g S_w)\phi \tag{A7}$$

ρ_w , ρ_g are the density of the water and gas, respectively.

The Mavko-Jizba relations use the bulk modulus K_{uf} and shear modulus μ_{uf} of the unrelaxed frame to replace the K_d and μ_d in the Gassmann equations (Eq. (A3) and (A4)) to calculate the moduli of the fully saturated sample ($K_{MJ} = K$; $\mu_{MJ} = \mu = \mu_{uf}$) and the corresponding velocities by Eq. (A1) and (A2).

$$\frac{1}{K_{uf}} \approx \frac{1}{K_h} + (\frac{1}{K_f} - \frac{1}{K_s})\phi_s \tag{A8}$$

$$(\frac{1}{\mu_{uf}} - \frac{1}{\mu_d}) = \frac{4}{15}(\frac{1}{K_{uf}} - \frac{1}{K_d}) \tag{A9}$$

ϕ_s: soft porosity or the porosity that closes at high pressure; $\phi_s = \phi/50$ is used in the simulation. K_h: effective bulk modulus of dry sample at high pressure when the soft porosity is compressed to close; $K_h = \pi K_d$ is used in the simulation. As the $K_d \propto P^{\frac{1}{3}}$ according to the Hertz-Mindlin theory, the K_h is approximated to the bulk modulus of the dry granular glassbead packing under confining pressure $P \approx 0.15 \times \pi^3 \approx 5\ MPa$, which is a reasonable confining pressure to suppress the soft porosity.

Appendix B Attenuation Estimation by Spectral-Ratio Method

The P- and S-wave attenuation (inverse quality factor) in glass bead packings are calculated by the spectral-ratio method (Toksöz et al., 1979). The ratio of amplitudes for the reference aluminum core and the sample is given as

$$\ln\left(\frac{A_1}{A_2}\right) = (\gamma_2 - \gamma_1)Lf + \ln\left(\frac{G_1}{G_2}\right), \tag{B1}$$

where A is the Fourier amplitude, γ is the attenuation coefficient, f is the frequency, and G denotes the geometrical spreading factor. Subscripts 1 and 2 indicate the sample and reference, respectively. $\ln(G_1/G_2)$ is a constant due to the sample and reference have the same shape and size. The sample length L and can be obtained from the direct measurement. The quality factor Q related to the attenuation coefficient can be expressed as

$$Q = \frac{\pi}{\gamma v}, \tag{B2}$$

where v is the phase velocity. Since Q of the reference sample is very high, γ_2 can be considered as 0, which only introduces an error of less than 1%. Thus, Eq. (B1) can be written as

$$\ln\left(\frac{A_1}{A_2}\right) = \frac{-\pi L}{Q_1 v} + \ln\left(\frac{G_1}{G_2}\right). \tag{B3}$$

The attenuation of sample (Q_1^{-1}) can be estimated from the slope of the linear fitting of $\ln\left(\frac{A_1}{A_2}\right)$ versus the frequency.

Acknowledgments

This study was supported by an Australian Government Research Training Program (RTP) Scholarship. J. Li thanks Dr. Faaiz Al-Shajalee for the microscopy images and Dr. Nilesh Kumar for the training of IFT and contact angle measurements. T. Müller acknowledges the support of the Jiangsu 100 Plan of Foreign Experts.

Data availability: The waveform data are available at: https://doi.org/10.5281/zenodo.4665478.

References

Alemu, B. L., Aker, E., Soldal, M., Johnsen, Ø., & Aagaard, P. (2013). Effect of sub-core scale heterogeneities on acoustic and electrical properties of a reservoir rock: a co2 flooding experiment of brine saturated sandstone in a computed tomography scanner. *Geophysical Prospecting*, *61*(1), 235–250.

Anderson, W. G. (1987). Wettability literature survey part 5: The effects of wettability on relative permeability. *Journal of Petroleum Technology*, *39*(11), 1453–1468.

Anderson, W. G., et al. (1986). Wettability literature survey-part 1: rock/oil/brine interactions and the effects of core handling on wettability. *Journal of petroleum technology*, *38*(10), 1–125.

Anderson, W. G., et al. (1987a). Wettability literature survey-part 4: Effects of wettability on capillary pressure. *Journal of petroleum technology*, *39*(10), 1–283.

Anderson, W. G., et al. (1987b). Wettability literature survey-part 6: the effects of wettability on waterflooding. *Journal of petroleum technology*, *39*(12), 1–605.

Anthony, J. L., & Marone, C. (2005). Influence of particle characteristics on granular friction. *Journal of Geophysical Research: Solid Earth*, *110*(B8).

Ba, J., Carcione, J., & Nie, J. (2011). Biot-rayleigh theory of wave propagation in double-porosity media. *Journal of Geophysical Research: Solid Earth*, *116*(B6).

Berryman, J. G., & Thigpen, L. (1985). Effective constants for wave propagation through partially saturated porous media. *Applied Physics Letters*, *46*(8), 722–724.

Brunet, T., Jia, X., & Mills, P. (2008). Mechanisms for acoustic absorption in dry and weakly wet granular media. *Physical review letters*, *101*(13), 138001.

Bultreys, T., Van Hoorebeke, L., & Cnudde, V. (2016). Simulating secondary waterflooding in heterogeneous rocks with variable wettability using an image-based, multiscale pore network model. *Water Resources Research*, *52*(9), 6833–6850.

Cadoret, T., Marion, D., & Zinszner, B. (1995). Influence of frequency and fluid distribution on elastic wave velocities in partially saturated limestones. *Journal of Geophysical Research: Solid Earth*, *100*(B6), 9789–9803.

Daniels, K. E., & Hayman, N. W. (2008). Force chains in seismogenic faults visualized with photoelastic granular shear experiments. *Journal of Geophysical Research: Solid Earth*, *113*(B11).

Davis, R. H., Serayssol, J.-M., & Hinch, E. (1986). The elastohydrodynamic collision of two spheres. *Journal of Fluid Mechanics*, *163*, 479–497.

Dutta, N., & Odé, H. (1979). Attenuation and dispersion of compressional waves in fluid-filled porous rocks with partial gas saturation (white model)—part ii: Results. *Geophysics*, *44*(11), 1789–1805.

Dutta, T., Mavko, G., & Mukerji, T. (2010). Improved granular medium model for unconsolidated sands using coordination number, porosity, and pressure relations. *Geophysics*, *75*(2), E91–E99.

Dvorkin, J., Mavko, G., & Nur, A. (1991). The effect of cementation on the elastic properties of granular material. *Mechanics of Materials*, *12*(3-4), 207–217.

Dvorkin, J., Nur, A., & Yin, H. (1994). Effective properties of cemented granular materials. *Mechanics of materials*, *18*(4), 351–366.

Garrouch, A. A., & Alikhan, A. A. (1997, 06). *An Improved Method For Quantifying In-Situ Intermediate Wettability Using Well Logs* (Vol. All Days). (SPWLA-1997-Z)

Garrouch, A. A., & Sharma, M. M. (1995). Dielectric properties of partially saturated rocks. *Energy & Fuels*, *9*(3), 413-419. doi: 10.1021/ef00051a004

Griffiths, S., Rescaglio, A., & Melo, F. (2010). Ultrasound propagation in wet and airless non-consolidated granular materials. *Ultrasonics*, *50*(2), 139–144.

Güven, I., Luding, S., & Steeb, H. (2018). Incoherent waves in fluid-saturated sintered granular systems: Scattering phenomena. *Journal of vibration and acoustics*, *140*(1).

Howell, D., Behringer, R. P., & Veje, C. (1999). Stress fluctuations in a 2d granular couette experiment: a continuous transition. *Physical Review Letters*, *82*(26), 5241.

Hu, R., Wan, J., Kim, Y., & Tokunaga, T. K. (2017). Wettability impact on supercritical co2 capillary trapping: Pore-scale visualization and quantification. *Water Resources Research*, *53*(8), 6377–6394.

Jia, X., Caroli, C., & Velicky, B. (1999). Ultrasound propagation in externally stressed granular media. *Physical Review Letters*, *82*(9), 1863.

Job, S., Santibanez, F., Tapia, F., & Melo, F. (2008). Nonlinear waves in dry and wet hertzian granular chains. *Ultrasonics*, *48*(6-7), 506–514.

Johnson, D. L. (2001). Theory of frequency dependent acoustics in patchy-saturated porous media. *The Journal of the Acoustical Society of America*, *110*(2), 682–694.

Johnson, P. A., & Jia, X. (2005). Nonlinear dynamics, granular media and dynamic earthquake triggering. *Nature*, *437*(7060), 871–874.

Khishvand, M., Alizadeh, A., Kohshour, I. O., Piri, M., & Prasad, R. (2017). In situ characterization of wettability alteration and displacement mechanisms governing recovery enhancement due to low-salinity waterflooding. *Water Resources Research*, *53*(5), 4427–4443.

Ladd, C. R., & Reber, J. E. (2020). The effect of a liquid phase on force distribution during deformation in a granular system. *Journal of Geophysical Research: Solid Earth*, *125*(8), e2020JB019771.

Langlois, V., & Jia, X. (2014). Acoustic probing of elastic behavior and damage in weakly cemented granular media. *Physical Review E*, *89*(2), 023206.

Lebedev, M., Toms-Stewart, J., Clennell, B., Pervukhina, M., Shulakova, V., Paterson, L., ... Wenzlau, F. (2009). Direct laboratory observation of patchy saturation and its effects on ultrasonic velocities. *The Leading Edge*, *28*(1), 24–27.

Liu, C.-h., & Nagel, S. R. (1992). Sound in sand. *Physical review letters*, *68*(15), 2301.

Liu, J., Müller, T. M., Qi, Q., Lebedev, M., & Sun, W. (2016). Velocity-saturation relation in partially saturated rocks: Modelling the effect of injection rate changes. *Geophysical Prospecting*, *64*(4-Advances in Rock Physics), 1054–1066.

Lo, W.-C., & Sposito, G. (2013). Acoustic waves in unsaturated soils. *Water Resources Research*, *49*(9), 5674–5684.

Lo, W.-C., Sposito, G., & Majer, E. (2005). Wave propagation through elastic porous media containing two immiscible fluids. *Water Resources Research*, *41*(2).

Lo, W.-C., Yang, C.-C., Hsu, S.-Y., Chen, C.-H., Yeh, C.-L., & Hilpert, M. (2017). The dynamic response of the water retention curve in unsaturated soils during drainage to acoustic excitations. *Water Resources Research*, *53*(1), 712–725.

Lopes, S., Lebedev, M., Müller, T. M., Clennell, M. B., & Gurevich, B. (2014). Forced imbibition into a limestone: Measuring p-wave velocity and water saturation dependence on injection rate. *Geophysical Prospecting*, *62*(5), 1126–1142.

Makse, H. A., Gland, N., Johnson, D. L., & Schwartz, L. (2004). Granular packings: Nonlinear elasticity, sound propagation, and collective relaxation dynamics. *Physical Review E*, *70*(6), 061302.

Mavko, G., & Jizba, D. (1991). Estimating grain-scale fluid effects on velocity dispersion in rocks. *Geophysics*, *56*(12), 1940–1949.

Mavko, G., & Mukerji, T. (1998). Bounds on low-frequency seismic velocities in partially saturated rocks. *Geophysics*, *63*(3), 918–924.

Melosh, H. (1996). Dynamical weakening of faults by acoustic fluidization. *Nature*, *379*(6566), 601–606.

Moebius, F., Canone, D., & Or, D. (2012). Characteristics of acoustic emissions induced by fluid front displacement in porous media. *Water Resources Research*, *48*(11).

Mukerji, T., Mavko, G., Mujica, D., & Lucet, N. (1995). Scale-dependent seismic velocity in heterogeneous media. *Geophysics*, *60*(4), 1222–1233.

Müller, T. M., & Gurevich, B. (2004). One-dimensional random patchy saturation model for velocity and attenuation in porous rocksradom patchy saturation model. *Geophysics*, *69*(5), 1166–1172.

Murphy III, W. F. (1984). Acoustic measures of partial gas saturation in tight sandstones. *Journal of Geophysical Research: Solid Earth*, *89*(B13), 11549–11559.

Nagy, P. B., & Blaho, G. (1994). Experimental measurements of surface stiffness on water-saturated porous solids. *The Journal of the Acoustical Society of America*, *95*(2), 828–835.

Owens, E. T., & Daniels, K. E. (2011). Sound propagation and force chains in granular materials. *EPL (Europhysics Letters)*, *94*(5), 54005.

Parra, J. O., Hackert, C. L., & Bennett, M. W. (2006). Permeability and porosity images based on p-wave surface seismic data: Application to a south florida aquifer. *Water Resources Research*, *42*(2).

Qi, Q., Müller, T. M., Gurevich, B., Lopes, S., Lebedev, M., & Caspari, E. (2014). Quantifying the effect of capillarity on attenuation and dispersion in patchy-saturated rocks. *Geophysics*, *79*(5), WB35–WB50.

Rolo, L. I., Caco, A. I., Queimada, A. J., Marrucho, I. M., & Coutinho, J. A. (2002). Surface tension of heptane, decane, hexadecane, eicosane, and some of their binary mixtures. *Journal of Chemical & Engineering Data*, *47*(6), 1442–1445.

Santos, J. E., Douglas Jr, J., Corberó, J., & Lovera, O. M. (1990). A model for wave propagation in a porous medium saturated by a two-phase fluid. *The Journal of the Acoustical Society of America*, *87*(4), 1439–1448.

Sayers, C., & Dahlin, A. (1993). Propagation of ultrasound through hydrating cement pastes at early times. *Advanced Cement Based Materials*, *1*(1), 12–21.

Sayers, C. M. (2021). Mechanical properties of grain contacts in unconsolidated sands. *Geophysics*, *86*(2), MR95–MR103.

Scott, D. R. (1996). Seismicity and stress rotation in a granular model of the brittle crust. *Nature*, *381*(6583), 592–595.

Sun, W., Xiong, F., Ba, J., & Carcione, J. M. (2018). Effects of ellipsoidal heterogeneities on wave propagation in partially saturated double-porosity rocks. *Geophysics*, *83*(3), WC71–WC81.

Toksöz, M., Johnston, D. H., & Timur, A. (1979). Attenuation of seismic waves in dry and saturated rocks: I. laboratory measurements. *Geophysics*, *44*(4), 681–690.

Toms, J., Müller, T., Ciz, R., & Gurevich, B. (2006). Comparative review of theoretical models for elastic wave attenuation and dispersion in partially saturated rocks. *Soil Dynamics and Earthquake Engineering*, *26*(6-7), 548–565.

Tserkovnyak, Y., & Johnson, D. L. (2003). Capillary forces in the acoustics of patchy-saturated porous media. *The Journal of the Acoustical Society of America*, *114*(5), 2596–2606.

White, J. (1975). Computed seismic speeds and attenuation in rocks with partial gas saturation. *Geophysics*, *40*(2), 224–232.

Xu, P., & Yu, B. (2008). Developing a new form of permeability and kozeny–carman constant for homogeneous porous media by means of fractal geometry. *Advances in water resources*, *31*(1), 74–81.